3. DOSIMETRY

G.S. HURST, R.H. RITCHIE, F.W. SANDERS, P.W. REINHARDT, J.A. AUXIER, E.B. WAGNER,
A.D. CALLIHAN AND K.Z. MORGAN
HEALTH PHYSICS DIVISION, OAK RIDGE NATIONAL LABORATORY,
OAK RIDGE, TENNESSEE, UNITED STATES OF AMERICA

3.1. Methods of dosimetry

The methods of dosimetry used for investigation of the doses received by the individuals exposed in the Yugoslav accident were essentially those used in connection with the Oak Ridge Y-12 accident [12, 13]. An outline of the general scheme is as follows: When fast neutrons enter the human body, most of these are moderated to thermal energy and a small fraction of these are captured by a (n, γ) process in Na^{23}, giving rise to Na^{24}, which by virtue of its emission of high-energy gamma rays with a half life of 14.8 h, is easily detected. It has been shown ([13], Fig. 1) that the probability of capture, making Na^{24}, is not a strong function of the energy of the fast neutrons and that the probability of capture for neutrons is higher in the fast region than in the thermal region. Thus, the uniform distribution of Na^{23} in the human body provides an excellent means of normalizing the neutron exposure of an individual. In particular, for a given neutron energy spectrum the fast neutron dose is proportional to the ratio Na^{24}/Na^{23} in the body or in the blood system. This method of normalization is quite important in the dosimetry of radiation accidents since no assumptions need be made about the exact location of an individual at the time of the energy release. The importance of this fact can be made clear by reference to the Y-12 accident [12] where it was shown by calculation of the neutron dose based on the known number of fissions and the stated location of the individual that one of the surviving individuals would have received a dose several times the lethal value. Thus, little credence can be placed in calculations requiring such assumptions.

More specifically, the determination of the neutron dose D_n and the gamma dose D_γ may be obtained from three quantities – $(D_n/a)_c$, $(D_\gamma/D_n)_c$, and a, which are related as follows:

$$D_n = (D_n/a)_c \times a$$

$$D_\gamma = (D_\gamma/D_n)_c \times D_n,$$

where the quantity $(D_n/a)_c$ is the neutron dose per unit of sodium activation which is characteristic of the type of source and the exposure conditions, a is the measured sodium activation of the individual, and $(D_\gamma/D_n)_c$ is the ratio of gamma dose to neutron dose which is characteristic of a given source and set of exposure conditions. In both the Y-12 and Vinča accident investigations the quantity $(D_n/a)_c$ was determined by two methods: experiment and theory. The experimental method at Vinča consisted in measurement of the neutron dose (with a Radsan fast neutron dosimeter [14]) required to produce a given amount of activation in a plastic man-shaped phantom filled with an aqueous solution of NaCl. The ratio $(D_\gamma/D_n)_c$ was determined with two types of gamma dosimeters [15, 16] and the Radsan neutron dosimeter. The quantity a was based on the Na^{24} analysis reported by Jammet *et al.* [6]. As a supplement and check on the experimental procedure, calculation of the quantities $(D_n/a)_c$ and $(D_\gamma/D_n)_c$ was made for the zero-power reactor. In addition to ascertaining the quantities D_γ and D_n, it is desirable to determine the neutron spectrum $N(E)$. This was done by calculation and by experiment with the series of threshold detectors [17, 18] developed for this purpose.

3.2. Experimental investigations

To accomplish the measurements indicated above, the zero-power reactor (Fig. 1) was operated in two different ranges of power level, which for convenience will be referred to as "low" power and "high" power. Fig. 16 shows the general location of the dosimetry equipment for the low- and high-power runs. The LPS stations show locations where most of the dose measurements were made; the V.T. and H.T. represent, respectively, locations where vertical and horizontal traverses were made with Au and S detectors during the high-power runs. Figs. 17a and 17b show the location of the phantoms for high-power runs at 1 kW and 5 kW respectively. For facilitation of intercomparison of data obtained from the two types of operating conditions, a sulphur pellet was placed at a convenient location on the side of the reactor tank before each run.

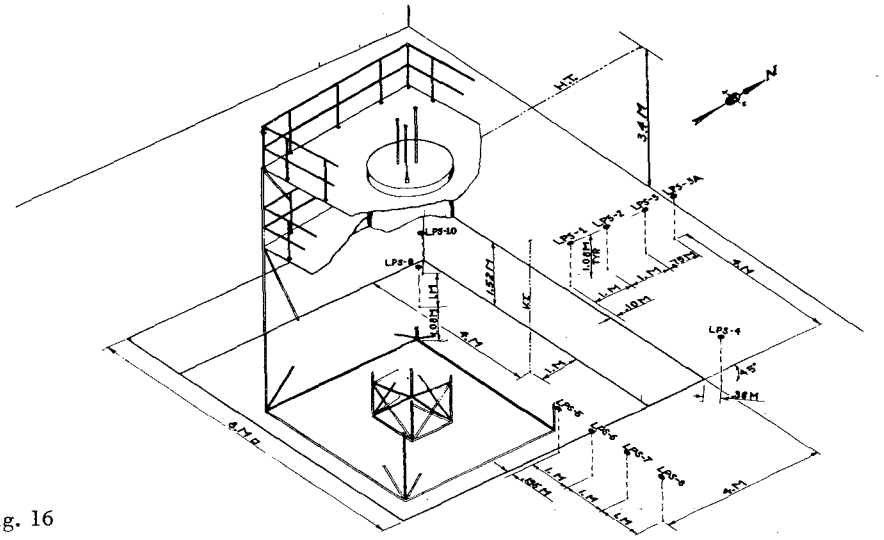

Fig. 16

Dosimetry stations in reactor room

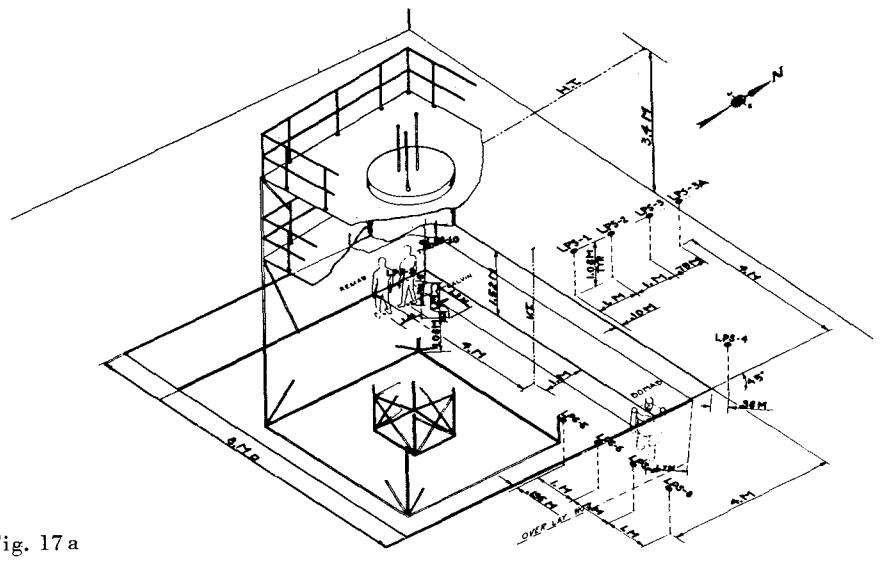

Fig. 17a

Dosimetry stations and phantom locations in reactor room during the 1-kW run

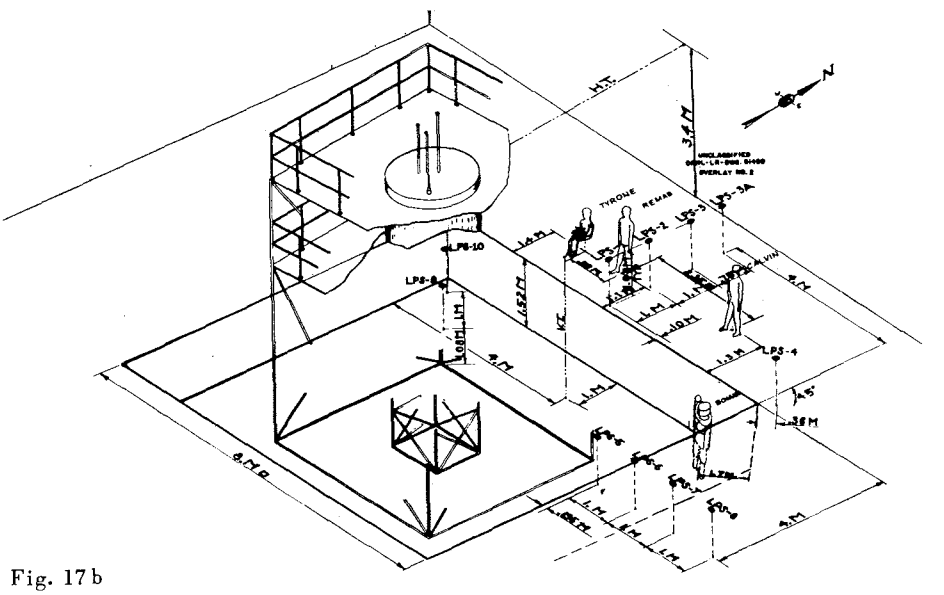

Fig. 17b

Dosimetry stations and phantom locations in reactor room during the 5-kW run

3.2.1. LOW-POWER EXPERIMENT

The ratio of gamma dose to fast neutron dose was measured at some of the positions shown in Fig. 16, with the equipment mentioned above (mounted as shown in Fig. 18) and with the reactor operating at a power level of approximately 5 W.* The results of the directly measured ratio $D\gamma/D_n$ are shown in Table II, which gives also the neutron dose, as measured with Radsan, per unit monitor flux density (i.e., sulphur neutrons/cm^2). The final D_γ/D_n values for the various positions are based on the counting method of gamma-ray dosimetry described in [15]. The carbon-CO_2 chamber [16] used in this experiment gave results which were 1.3 times the dose values obtained with the counting method, but later studies with the carbon-CO_2 chamber at ORNL showed that it has an appreciable response to thermal neutrons.

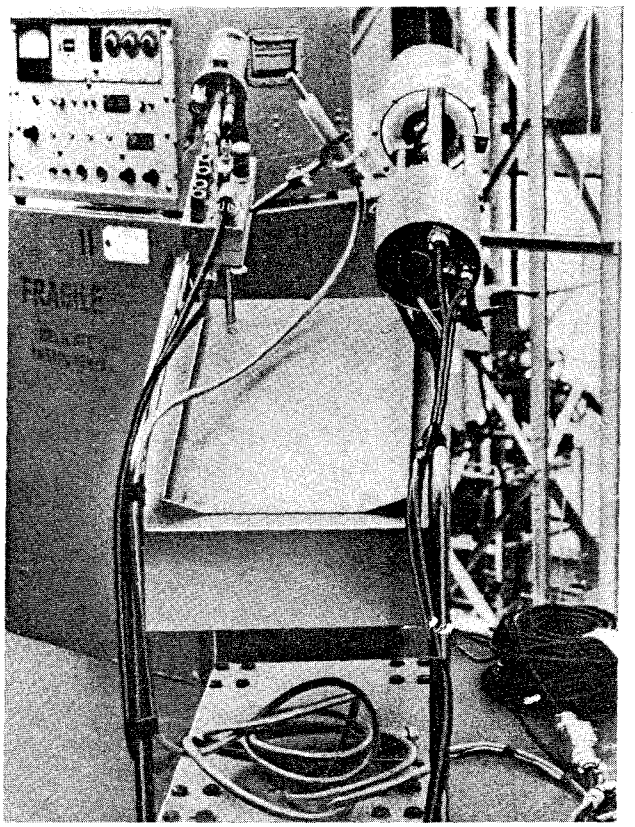

Fig. 18
Mounting arrangement for the low level dosimeters

TABLE II

EXPERIMENTAL VALUES FOR D_γ/D_n AT VARIOUS POSITIONS

Position	Neutron dose per unit monitor (rad/n cm^{-2})	$D\gamma/D_n$
1	1.13×10^{-6}	3.5
2	0.90×10^{-6}	3.6
3	0.75×10^{-6}	3.6
3a	0.66×10^{-6}	3.9
4	0.64×10^{-6}	3.8
8	0.54×10^{-6}	3.5
9	0.86×10^{-6}	4.0
10	0.72×10^{-6}	4.2

* *Private communication with D. Popović indicated that the power calibration in the initial run yielded a figure approximately 0.56 times the value quoted here. This correction factor applies to all power levels quoted in the remainder of this report.*

3.2.2. HIGH-POWER EXPERIMENT

With the reactor operating first at 1 kW and then at 5 kW, two types of measurements were made: neutron spectrum measurements and Na^{24} activation in man-shaped phantoms. The spectral measurements were made with threshold detectors [17, 18] located at various positions (stations). The results obtained for Stations 1, 9 and 10 are shown in Table III, where comparison is made with the spectral data obtained for the Y-12 excursion with the same type of detector.

TABLE III

EXPERIMENTAL INFORMATION ON NEUTRON SPECTRUM
(Ratio of flux above threshold of various detectors to total fast flux)

Sample	Boris Kidrič (ZPR) threshold energy			Y-12 excursion
	Station 1	Station 9	Station 10	
Pu	1.00	1.00	1.00	1.00
Np	0.36	0.35	0.35	0.89
U	0.20	0.18	0.19	0.54
S	0.094	0.088	0.090	0.25
Au	3.91	3.63	3.87	0.45

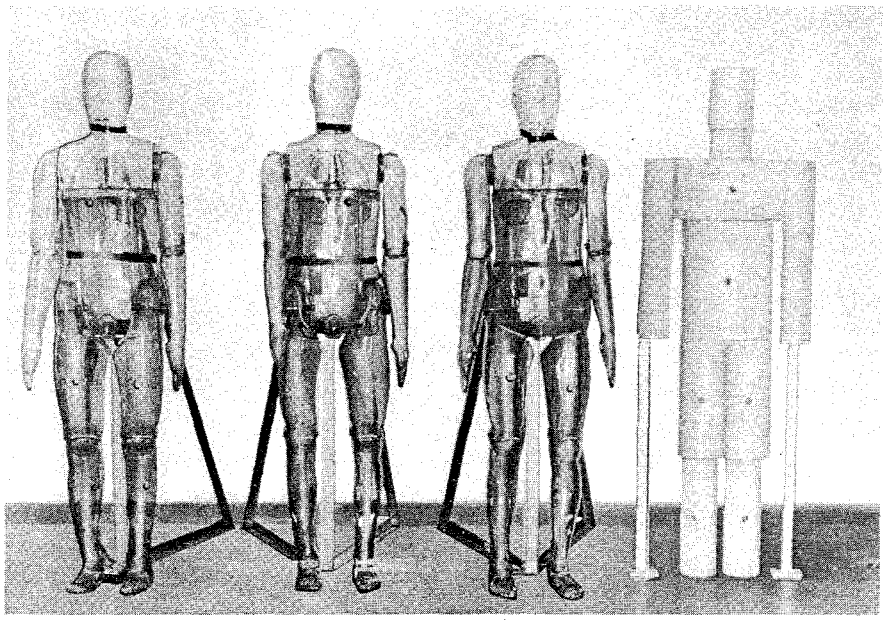

Fig. 19

The four plastic phantoms. From left to right: Calvin, Remab, Tyrone and Bomab

Sodium activation data were obtained by location of phantoms (Fig. 19) at the positions shown in Fig. 16. During the 1-kW run the phantoms were located as shown in Fig. 17a, and during the 5-kW run they were located as shown in Fig. 17b. The phantoms were filled with an aqueous solution of NaCl at a concentration of 15.7 mg Na per gram of solution. After irradiation the sodium activation a (in units of μc Na^{24}/mg Na) was determined according to the technique described in ORNL-2748A [19]. From the data obtained during the low-power experiment, Table II, and from normalizing of the relative exposure in some cases by means of the activation of sulphur pellets placed on the phantoms, the neutron dose received by the phantoms was obtained. The results of $(D_n/a)_c$ are shown in Table IV, where each entry corresponds to the weighted

TABLE IV

NEUTRON DOSE PER UNIT SODIUM ACTIVATION FOR MAN-SHAPED PHANTOMS EXPOSED AT THE ZERO POWER REACTOR

Phantom	$(D_n/a)_C$ (rad μc^{-1} mg Na)	
	1-kW run	5-kW run
Tyrone	9.12×10^4	7.73×10^4
Remab	8.57×10^4	8.13×10^4
Calvin	9.12×10^4	7.27×10^4
Grand average = 8.65×10^4		

average value of a for all the compartments of the phantom. Further experimental data are given in Appendices 3A, 3B, 3C and 3D. In particular, Appendix 3B justifies the specific way in which the phantoms were used in this experiment. The concentration of sodium chloride used in the phantoms was nearly ten times that in the human body for the purpose of increasing the amount of Na^{24} for counting. In general, the sodium activation per mg of sodium would be less with a concentrated solution owing to capture of some of the available neutrons by chlorine nuclei. The neutron spectrum in the present experiment, however, contained a large proportion of low energy neutrons, most of which are reflected from the surface of the body. In such circumstances, an increase in the number of capturing nuclei in a phantom only reduces the proportion of reflected neutrons: the number of neutrons available for capture by sodium is effectively unchanged. The effect of increased concentration of sodium chloride was small in comparison with other uncertainties.

3.3. Theoretical investigations

In this section is given a description of the methods used in the calculation of neutron and gamma leakage from the Boris Kidrič zero-power reactor in the critical and near-critical state. The methods used are entirely theoretical in the sense that they rely not at all upon measurements which were made at Vinča. Multiple scattering of leakage radiation in walls and structure of the reactor building are neglected, and only direct leakage of neutrons and gamma rays from the assembly is considered. As shown below by comparison with experimental data, this approximation is surprisingly good although the agreement may be fortuitous in some particulars.

The quantities presented are: (1) $N_n(E)$, the neutron leakage spectrum: (2) $D_n(E)$, the neutron first collision dose leakage spectrum; (3) D_n/a, the ratio of the total first collision dose received by an idealized phantom to the Na^{24} activation generated in it by the leakage spectrum incident upon it; and (4) D_γ, the gamma-ray first collision dose leaking from the reactor due to the fission process and due to various neutron capture processes occurring in and around the reactor.

The method of computation of the neutron leakage which has been used in this work is the multigroup-diffusion approach. An existing criticality code written for the IBM-704, which automatically computes neutron leakage in several energy ranges, has been employed. The computation time for this code is quite modest for most systems. Gamma-ray leakage is treated by special IBM-704 codes. The method uses known gamma-ray cross-sections and buildup factors for calculation of attenuation kernels for the particular medium under consideration. The radiation field at various points inside or outside the assembly is then computed by summation over source points in the assembly, with the best estimates available for the gamma-ray spectra of the various sources. The spatial distribution of fissions in the assembly is obtained from the neutron leakage runs and is used in the gamma leakage calculation.

3.3.1. NEUTRON LEAKAGE SPECTRUM

The method which was employed for calculation of the neutron leakage spectrum from the Vinča reactor is based primarily upon the use of a multigroup, multiregion reactor analysis code [20] for the IBM-704. The basic equation solved by the code is the multigroup-diffusion approximation to the Boltzmann transport equation. The programme approximates the differential equation by a difference equation and allows as many as 250 space points and 44 energy groups in the solution of the resulting equations.

Since the Boris Kidrič reactor uses a lattice spacing which is quite small (12 cm) compared with the dimensions of the reactor, consideration of an equivalent homogenized reactor [21] should be a good approximation. The unit lattice cell was taken to be cylindrical with a fuel rod at its centre and containing the same quantity of D_2O as the real unit lattice cell. A preliminary multigroup calculation of the distribution of flux inside this cell was made, with the boundary condition of zero total current at the outer boundary of the equivalent cylindrical cell. Homogenized multigroup cross-sections were computed with the calculated flux distribution as a weighting function. A multigroup calculation of the escape spectrum for the entire reactor was then made with these cross-sections, with the assumption that a 1-cm layer of aluminium surrounded the volume. Fig. 20 shows a plot of the multiplication factor k of the assembly as a function of height. On the same graph is shown the total neutron leakage per fission neutron in the core as a function of height. This calculation predicts a critical height of approximately 185 cm, as compared with the experimental value [3] of 177.6 cm. It is felt that the agreement is sufficiently accurate for our purposes, since the neutron leakage varies by only approximately 4% over the range of heights. Backscattering of neutrons from the tank supporting members and from the walls of the room might well account for the difference between experimental and calculated values of the critical height. These results also show that there is negligible difference between neutron leakage per fission neutron in the critical state and in the delayed supercritical state which obtained at the time of the accident. Estimates of the $k_{ex} = k - 1$ appropriate to the excursion [5] show that $k_{ex} \simeq 10^{-3}$. According to Fig. 20, the neutron leakage per core neutron at this value of k_{ex} is only approximately 2% different from that in the steady state.* Hence, this difference will be neglected in the remainder of this calculation.

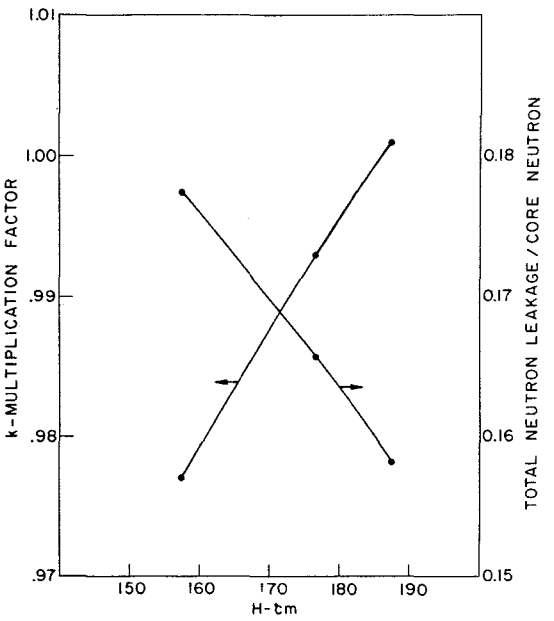

Fig. 20

Multiplication factor and total neutron leakage as a function of height

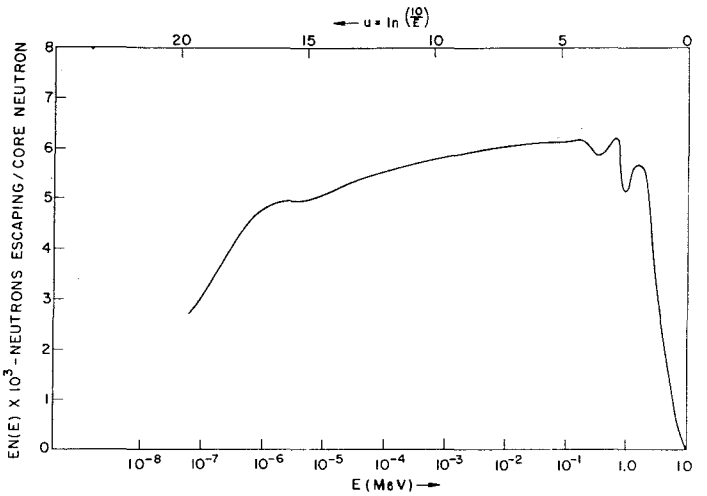

Fig. 21

Escape neutron spectrum

* *A change in the leakage per fission neutron with k would not by itself affect the result of this dosimetry study. A radical change in the neutron spectrum, on the other hand, would produce a change in the ratio of D_n/a and would mean that experimental work with a steady operating reactor would not be comparable with conditions obtaining during the accident. However, comparison of the calculations at different values of k indicates negligible change in the spectrum between the two reactor states.*

Fig. 21 shows the neutron leakage spectrum calculated for the reactor at the critical level * [22]. The quantity plotted in the ordinate is $EN(E)$, and the abscissa gives both the energy E and the lethargy $u = \ln \frac{10}{E(\mathrm{MeV})}$. The spectrum is conveniently represented in this way since the number of neutrons escaping between any two energies is just proportional to the area under the portion of the curve between these energies. The total fast leakage in this spectrum is 0.234 neutron per fission while the leakage in the thermal group is 0.157 neutron per fission.

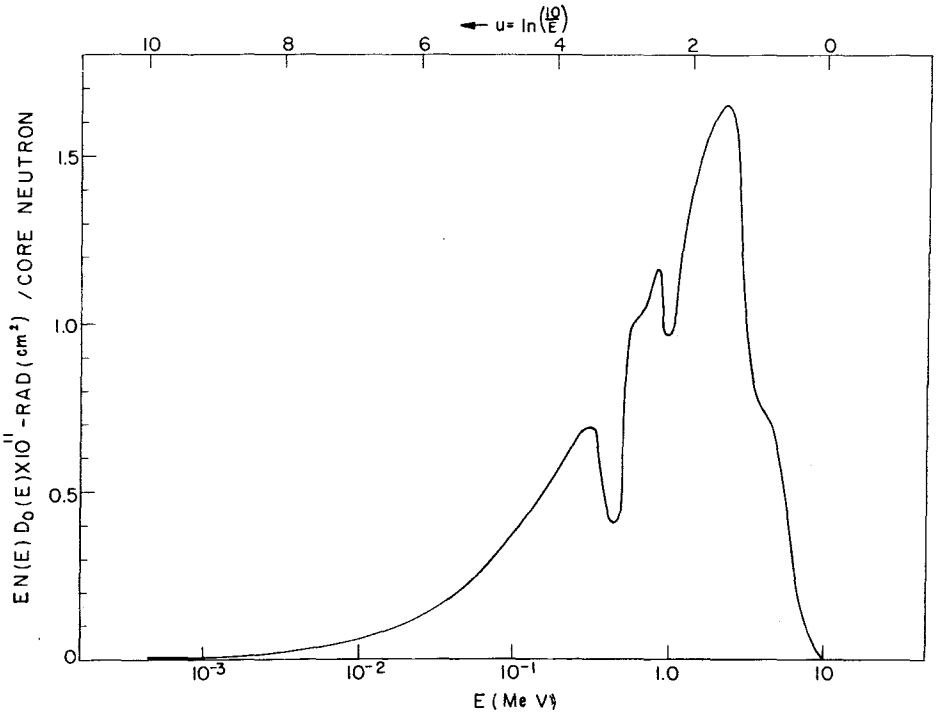

Fig. 22

Dose spectrum leaking from reactor

The first collision dose spectrum is shown in Fig. 22. The factor $D_0(E)$ is the first collision dose per unit neutron flux [23]. $\int D_0(E)\ N(E)\mathrm{d}E$ is found to be 4.37×10^{-11} $\frac{\text{rad cm}^2}{\text{core neutron}}$.

To make possible a comparison with experimental measurements of D_n, a calculation of $(D_n)_R \equiv \equiv \int D_{\mathrm{Radsan}}(E)\ N(E)\mathrm{d}E$ was carried out. $D_{\mathrm{Radsan}}(E)$ is the dose measured by the Radsan fast neutron dosimeter at energy E and is less than $D_0(E)$ at low energies due to bias losses. Values of $D_{\mathrm{Radsan}}(E)$ were inferred from the work of WAGNER and HURST [24]. The result of this calculation was $(D_n)_R = 3.12 \times 10^{-11}$ rad cm² per core neutron.

For calculation of a, the Na^{24} activation induced in a man exposed to the calculated spectrum, use was made of approximate results for $\xi(E)$ [13], the capture probability at thermal energy per unit flux of neutrons incident normal to the axis of a circular cylinder of 15 cm radius. Using the function $\xi(E)$, the quantity $(D_n)_R/a$ was calculated from

$$\frac{(D_n)_R}{a} = 1.12 \times 10^{11} \frac{\int D_0(E)\ N(E)\mathrm{d}E}{\int \xi(E)\ N(E)\mathrm{d}E} \quad \frac{\text{rad}}{\mu\text{c gm of Na}^{23}} = 7.2 \times 10^4 \quad \frac{\text{rad}}{\mu\text{c (mg Na)}^{-1}}$$

and compares favourably with the average value of 8.65×10^4 rad/μc(mg Na)$^{-1}$ obtained with the phantoms (see Table IV).

* *This spectrum is somewhat different in the low-energy range from a preliminary result given elsewhere (R.H. RITCHIE, H.B. ELDRIDGE, and V.E. ANDERSON, International Symposium on Selected Topics in Radiation Dosimetry, Vienna, Austria, June 1960). Improved values of the homogenized multigroup cross-sections were used in the present calculation* [22].

The multigroup computation of the leakage spectrum takes into account the neutron distribution in only one spatial dimension and introduces an artificial absorption to account for the leakage transverse in the direction in which computation proceeds. Within the framework of multigroup diffusion theory, one may take into account the dependence of the leakage flux on direction with respect to the reactor axis [22]. This has been done in the comparisons given in Table V.

TABLE V

SUMMARY OF $4\pi R^2 \times$ DOSE DUE TO VARIOUS SOURCES

Gamma Source	$D_\gamma \times 10^{10}$ - r cm^2/fission		
	Station 1	Station 9	Station 10
Prompt fission	1.77	1.46	1.63
U^{238} (n, γ) U^{239} capture	0.77	0.63	0.69
Moderator capture	0.05	0.05	0.05
Tank 2nd structure capture	~ 0.30	~ 0.30	~ 0.30
Fission products during experiment	1.12	0.92	1.03
Total dose during experiment	4.01	3.36	3.70
Fission products during accident	0.39	0.32	0.36
Total dose during accident	3.28	2.76	3.03
	Dose ratios (r/rad)		
$D_\gamma/(D_n)_R$ calculated for experiment	3.52	3.00	3.40
$D_\gamma/(D_n)_R$ measured for experiment	3.5	4.0	4.2
$D_\gamma/(D_n)_R$ calculated for accident	2.88	2.46	2.78
	$(D_n)_{Radsan} \times 10^{10}$ - rad cm^2/fission		
Leakage neutrons	1.14	1.12	1.09

Other comparisons which can be made between experiment and the calculation of the leakage spectrum are in the activation of the threshold detectors which were exposed during the work at Vinča. Table VI shows a comparison of various ratios calculated from the spectrum given above with experimental determinations of these ratios. The experimental values represent station averages. The quantity $\phi_{>E_T}$ represents the neutron flux lying above the effective energy threshold of E_T MeV in the case of various detectors. The quantity $4\pi R^2(D_n)_R/F$ was obtained from the experimental data by the use of the Radsan-measured neutron dose rate together with the fission rate F occurring inside the assembly. The latter value was obtained from a power calibration performed by the Yugoslav experimenters [25]. For comparison with experiment, the theoretical values have been corrected, approximately, for the non-$1/R^2$ variation of the dose at points in the neighbourhood of the reactor.

3.3.2. GAMMA-DOSE LEAKAGE

There are many sources of gamma radiation in and around the reactor which should be considered. Reasonably good estimates of the dose from most of them may be made. Although the uncertainties in these estimates are likely to be approximately 20%, it is clearly worth-while to make such calculations in order to understand better the physics of the accident. Each of the sources of gamma radiation will be considered in turn with detailed description relegated to appendices.

TABLE VI

COMPARISON OF CALCULATED AND EXPERIMENTAL DOSE AND FLUX RATIOS

Ratios	Experiment	Theory
$\frac{(D_n)_R}{\phi_{>2.5}} \times 10^8 \left(\frac{\text{rad cm}^2}{\text{neutron}}\right)$	1.6	1.55
$\frac{4\pi R^2 (D_n)_R}{F} \times 10^9 \left(\frac{\text{rad cm}^2}{\text{fission}}\right)$	0.90	0.77
$\frac{\phi_{>1.5}}{\phi_{>2.5}}$	2.1	2.32
$\frac{\phi_{>0.7}}{\phi_{>2.5}}$	3.8	3.84
$\frac{\phi_{>0.01}}{\phi_{>2.5}}$	11.3	15.6
Gold foil — cadmium ratio	3.5-6.5	4.9

3.3.2.1. *Prompt gamma rays from the fission process and capture gamma rays from the U^{238} $(n,\gamma)U^{239}$ process*

The distribution in energy of prompt fission gamma rays is taken from the work of MAIENSCHEIN *et al.* [26]. The energy distribution of gammas from the $U^{238}(n,\gamma)U^{239}$ process is taken from the work of BARTHOLOMEW and HIGGS [27]. To calculate the escape of these photons from the reactor, one must consider attenuation both in the uranium rods and in the D_2O. Some simplifying assumptions were made in order that leakage from this very inhomogeneous system could be estimated in a reasonably short computing time. For the purpose of calculating leakage the distribution of fissions in a given fuel rod was assumed to be flat in the radial direction and to depend only on position along the length of the rod. The attenuation of gammas in the fuel rod in which they originate is accounted for, but their attenuation in other fuel rods is neglected. This approximation should result in little error since the rods are small in diameter compared with the lattice pitch. The computation proceeds by a numerical integration of the product of the source strength and leakage probability for each element in the source. The photon source distribution is obtained from the neutron criticality calculation described above. The attenuation of photons in travelling from a given source point to a field point outside the reactor is calculated with tabulated photon attenuation coefficients [28] and infinite medium buildup factors for that part of the path lying inside the reactor. The error involved in the use of these buildup factors should be small in the cases which we shall consider. A more detailed description of the computational procedure is given in Appendix 3A.

The leakage probability is a function of the distance from the reactor and the angle which the vector to the field point makes with the axis of the reactor. The results for some of the stations are given in Table V and are expressed as $4\pi R^2$(dose/fission) at the respective stations, where R is the distance from the centre of the reactor to the various stations.

3.3.2.2. *Gamma rays from fission products*

The estimate of this contribution is uncertain due to the fact that it depends to some extent upon the movement of the exposed persons after the reactor scram. In view of the uncertainty this fraction of the total dose received was approximated. The attenuation kernel of fission-product gamma rays in the lattice was taken to be the same as that of prompt fission gammas; and, further, it was assumed that the first can be estimated by scaling of the second according to the relative energy released in the two processes. Details of this estimate are given in Appendix 3B, and Table V shows the results for Stations 1, 9, and 10 for two

different cases: (1) at 15 min after the beginning of a steady-power-level run (in this case the dose values should be interpreted as r/sec per fission/sec), and (2) 4 min after the beginning of an excursion with a doubling time of 10 sec. The dose values refer to the total fission-product gamma dose received during the interval per fission occurring.

3.3.2.3. *Gamma rays from capture in the moderator and fuel cladding*

The thermal utilization for the reactor was calculated by multigroup methods to be $f = 0.9865$ for an assumed concentration of 0.16% H_2O in the moderator. With the assumption that all of these captures occur in hydrogen nuclei and given that c, the moderator capture probability per fission in the critical state, is equal to $(1 - f)/b$, where b is the ratio of fission to total capture probability in the fuel, it follows that

$$c = \frac{1 - f}{b} = \frac{0.0135}{0.543} = 0.0349 \text{ moderator captures/fission.}$$

A calculation of the leakage of hydrogen capture gammas from the homogenized reactor gave $\sim 0.5 \times 10^{-10}$ rad cm^2/fission for the three stations considered (Table V). The same multigroup calculation showed the capture probability in the aluminium cladding around the fuel rods to be 0.00642 captures per total capture. The dose due to this source would be expected to be even smaller than that due to captures in the moderator, especially since attenuation of these photons in the fuel rod should make the effective source strength even smaller; thus it has been neglected in Table V.

3.3.2.4. *Gamma rays from capture in tank walls and supporting structure*

This source of photons is difficult to estimate accurately because of the very complicated configuration of materials, chiefly aluminium, in the immediate neighbourhood of the assembly. A rough estimate, assuming that the structural aluminium may be considered equivalent to a 2-cm layer enveloping the whole reactor, gives 3×10^{-10} r cm^2/fission in the region around the reactor.

3.3.2.5. *Gamma rays from capture in the walls and floor of the reactor room*

This contribution is very difficult to estimate with any accuracy and hence was not considered.

3.3.3. DISCUSSION

The chief uncertainties in the estimates given above are: (1) use of infinite medium buildup factors rather than those appropriate to a finite medium, (2) neglect of photon attenuation in rods other than that in which a given photon originates, and (3) neglect of photons from neutron capture in reactor room materials and in the air of the room. The net uncertainty in the calculation is estimated to be $\sim \pm 20$ %. The ratio of the gamma doses during the accident to corresponding doses during the experiment f should be more accurate than this, and consequently this ratio will be used for correction of the experimental data.

Table V also shows the neutron dose $(D_n)_{\text{Radsan}}$ at the three stations considered. We estimated these values by taking into account the angular distribution of radiation leaving the reactor and correcting for the finite size of the reactor by the use of a radiation centre displaced 0.8 m toward a given station from the centre of the reactor. Also shown in this table are the values of Dy/D_n inferred from the above estimates and a comparison of these values with those obtained during the experiment.

3.4. Assignment of individual doses

In previous evaluations of dose received by man, mainly because of the difficulty of specifying a dose within the body which would have the desired radiobiological significance, the usual procedure has been to evaluate the first collision dose for both neutrons and gamma radiation. This procedure has been justified on the basis that, if the first collision doses are determined along with certain additional exposure conditions (i.e., angular and spectral distribution of the incoming radiations), more elaborate correlations of medical effects and exposure doses may be carried out at future times when more detailed biological mechanisms are understood or are being tested. In the case of the Y-12 exposures, the first collision dose for gamma radiation and fast neutrons and the neutron and gamma-ray energy distributions are given. In the present case, however, it appears advisable to comment on the gamma radiation produced by the capture of low-energy neutrons by the H(n, γ) reaction. From the neutron spectrum (Section 3.3) and the calculations by SNYDER [29], it may be seen that the additional gamma dose near the surface of a 30-cm slab makes an appreciable contribution to the total dose at that point.

We separate the neutron exposure into two dose components, namely, (1) the first-collision charged-particle dose made up of thermal neutron interactions of the type $N^{14}(n, p)C^{14}$ and recoil atoms (H, C, N, O) from fast-neutron interactions, and (2) the autointegral gamma dose at the surface of the slab due to the $H(n, \gamma)D$ process.

At present there are not available data which enable one to calculate the $H(n, \gamma)D$ autointegral dose for a realistic model of a man bombarded with neutrons. However, there are data [29] on the autointegral dose in a slab due to normal irradiation by neutron beams of various energies. These data are conservative in the present connection; i.e., the doses obtained using these values will surely represent over-estimates of the autointegral doses to a man and may be too large by a factor of 2.

The surface autointegral doses per unit neutron flux in the slab case were used for calculation of the dose for the whole neutron spectrum, shown in Fig. 21. The result was found to be

$$[H(n, \gamma)D \text{ autointegral dose}]_I = 1.50 \text{ (charged particle dose)}_I .$$

It may be seen that

$$\text{(charged particle dose)}_I = (\mu c/\text{mg Na})_I \, (W_I/W_p)^{1/3} \left(\frac{\text{charged particle dose to phantom}}{\mu c/\text{mg Na in phantom}} \right),$$

where I refers to the individual case and $(W_I/W_p)^{1/3}$ is a correction factor based on the weight W. From the experimental data obtained on the Na^{24} activation in the phantoms (Section 3.2) it may be seen that

$$\left(\frac{\text{charged particle dose to phantom}}{\mu c/\text{mg Na in phantom}} \right) = 1.40 \times 8.65 \times 10^4 \text{ rad}/\mu c \text{ mg}^{-1} ,$$

where the factor 1.40 is a correction for the energy lost under the bias of the neutron dosimeter, as derived in Section 3.3.

The first collision gamma doses (external doses) for the individuals may be expressed as

$$(D_\gamma)_{G, D, B} = \frac{3.6}{1.4} \times 0.82 \text{ (charged particle dose)}_I$$

$$(D_\gamma)_{H, V, M} = \frac{4.1}{1.4} \times 0.82 \text{ (charged particle dose)}_I$$

where we have used the results of Table II for the quantities D_γ/D_n most appropriate to the individuals, and the factor 0.82 corrects the D_γ/D_n ratios as measured in the constant power reactor experiment to the values appropriate to the intensity time relationship for the accident.

Table VII shows the individual sodium activation as reported by JAMMET *et al.* [6], the weights of the individuals, and the magnitude of the factor $(W_I/W_p)^{1/3}$. The individual doses as determined by the equations above are shown in Table VIII.

TABLE VII

INDIVIDUAL SODIUM ACTIVATION AND RELATED DATA

Individual	Total Na^{24} (μc)	Weight (kg)	Na^{24} (μc/mg Na)	$(W_I/W_p)^{1/3}$
H	53	65	5.44×10^{-4}	1.00
V	82	80	6.83×10^{-4}	1.08
G	76	70	7.24×10^{-4}	1.03
M	75	72	6.94×10^{-4}	1.04
D	63	52	8.07×10^{-4}	0.93
B	45	90	3.33×10^{-4}	1.12
(Phantom)		65		

The main uncertainty in the dose values given in Table VIII is associated with the H(n, γ)D dose component. As already stated, this value may be too high by a factor of about 2; however, even in this case, the total dose would be decreased only by about 15%. The uncertainties associated with the other dose components are smaller: the standard deviations for the charged particle doses and for the external gamma doses are estimated to be ± 12 % and ± 14 %, respectively.

Work is now in progress on the study of Na^{24} activation in phantoms of various shapes and sizes and with neutrons of various energies. The question of biological elimination of Na^{24} is being investigated with living animals exposed at various dose levels. When these studies have been completed, it may be desirable to re-evaluate the individual doses received from the various radiation accidents, including the Y-12 (Oak Ridge) accident and the Yugoslavia accident.

TABLE VIII

INDIVIDUAL DOSES
(All values in Rad units)

Individual	Charged particle dose	H(n, γ)D gamma dose	Exposure gamma dose	Total
H	66	99	158	323
V	89	133	214	436
G	90	135	189	414
M	87	130	209	426
D	91	136	192	419
B	45	67	95	207

APPENDIX 3A

GAMMA-DOSE LEAKAGE COMPUTATIONS

3A.1. Computation of the leakage of gamma rays originating in fuel rods

The computation proceeds by a numerical evaluation of the following integral:

$$D_\gamma(\mathbf{R}) = \int d\mathbf{r}\, S(\mathbf{r}) \frac{d_\gamma(|\mathbf{P}|, \theta)}{4\pi (|\mathbf{R} - \mathbf{r}|)^2},$$

where R is a vector from the centre of the reactor to the field point where the leakage dose is desired, r is a vector from the reactor centre to the volume element dr where the gamma source strength is $S(\mathbf{r})$, p is the part of the vector R - r which lies inside the reactor volume, and θ is the angle between R and the cylinder axis. The source distribution function $S(\mathbf{r})$ is obtained from the neutron leakage calculation described above and is equal to the number of photons per fission times the normalized fission probability in the homogenized reactor.

The dose attenuation kernel $d_\gamma(\mathbf{r})$ is calculated by summing over the distribution of energies present in the particular source after weighting each energy component by an attenuation factor, which is calculated

with known absorption coefficients and buildup factors, and a self-absorption factor to account for fuel-rod attenuation. More specifically,

$$d_\gamma(r, \theta) = \int dE\, n_\gamma(E) \mathcal{D}_0(E)\, B\,[E, r\mu(E)] \times e^{-r\mu(E)} \mathcal{J}(E, \mu_r(E)a, \theta),$$

where r is the distance from an isotropic point source in an infinite D_2O medium, $\mathcal{D}_0(E)$ is the first collision dose in rad/photon $\times$ cm^{-2} delivered by photons of energy E, $\mu(E)$ is the mass absorption coefficient of the medium for photons of that energy, and $B[(E, r\mu(E)]$ is the buildup factor for photons in the medium. We have chosen to use infinite medium buildup factors even though the systems are bounded [30]. The error incurred in making this approximation should be approximately 10%.

The self-absorption factor $\mathcal{J}(E, \mu_r(E)\, a_0, \theta)$ is calculated by carrying out an integral over the cross-section of the rod at radius a_0, using attenuation coefficients $\mu_r(E)$ appropriate to natural uranium at the energy E and taking into account the angle θ which the direction of observation makes with the axis of the rod. Buildup factors for the part of the photon path lying inside the rod were taken to be appropriate to the same distance, measured in g/cm^2, in the D_2O medium, as suggested by GOLDSTEIN and WILKINS [31]. As mentioned in Section 3.3.2.1, rod attenuation of photons not originating in a particular rod is neglected since the rod radius is small in comparison with the lattice pitch.

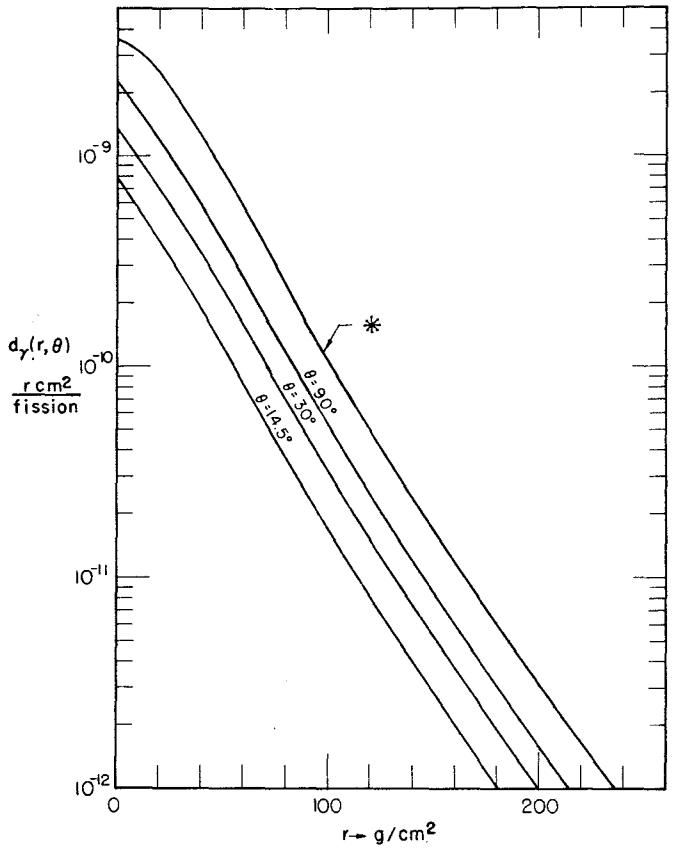

Fig. 23

Attenuation kernel for prompt-fission gamma-ray spectrum. Rod diameter = 2.54 cm.

* No rod absorption

Fig. 23 shows a graph of the attenuation kernel for the prompt fission gamma spectrum for the case of no rod absorption and for a natural uranium rod 1 in in diameter viewed at various angles with respect to the rod axis. Note that the curve labelled $\theta = 14.5°$ is probably too small in magnitude since the simple ray-path-length approach used here will surely break down at grazing angles relative to the rod axis. A "short-circuiting" effect will become important, i.e., photons emerging from the rod in directions nearly perpendicular to the axis may make collisions on D_2O molecules which will deflect them into directions nearly parallel with the rod axis. These photons may contribute in larger quantity than those taking longer paths through the rod. However, small values of θ are not required for the calculation of doses to any of the stations measured in the experiment.

TABLE IX

DOSE DUE TO PROMPT FISSION GAMMA RAYS AS A FUNCTION OF DISTANCE FROM REACTOR

	$4\pi R^2 D_\gamma$ - r cm^2/fission		
R (cm)	$\theta = 90°$	$\theta = 30°$	$\theta = 14.5°$
300	2.31×10^{-10}	1.21×10^{-10}	0.795×10^{-10}
400	2.21×10^{-10}	1.19×10^{-10}	0.743×10^{-10}
500	2.16×10^{-10}	1.19×10^{-10}	0.715×10^{-10}
600	2.12×10^{-10}	1.18×10^{-10}	0.697×10^{-10}

Table IX shows values of $4\pi R^2 D_\gamma$ vs R for three different viewing angles θ and for the prompt fission gamma source distribution.

3A.2. Estimate of fission-product gamma contribution to the total dose

The rate of energy release by fission products may be taken to be the following function of time [32]:

$$E(t) = \frac{0.62}{1+t} \quad \frac{\text{MeV}}{\text{sec/fission}},$$

where t is in sec and $t \leq 1\,000$ sec. For comparison, the total photon energy released in prompt fission was taken to be 7.2 MeV [32].

First, R_s, the ratio of photon energy released per unit time by fission products to the prompt fission rate at the end of approximately 15 min of steady operation is given by

$$R_s = \frac{1}{7.2\ \text{MeV}} \times 0.62 \int_0^{900} \frac{dt}{1+t}\ \text{MeV} \simeq \frac{0.62}{7.2} \ln 900 = 0.586,$$

and this ratio should have obtained at the time measurements of the gamma dose rate were made during the experiment.

Next, R_a, the ratio of total photon energy released by fission products in a time T, during which the reactor is critical on a 10-sec doubling time*, to the prompt fission gamma energy released may be shown to be

$$R_a = \frac{1}{7.2\ \text{MeV}} \times \frac{0.62}{t_0(1 - e^{-T/t_0})} \int_0^T e^{-\tau/t_0} \ln(1 + t - \tau)\, d\tau,$$

where $t_0 = 10$ sec/0.693. For an operating time T of 4 min [33], the above expression is closely equal to

$$R_a = \frac{0.62}{7.2} e^{1/t_0} E_1(1/t_0).$$

Numerical evaluation of these quantities, with values from the data of [22], gave the more accurate values of $R_S = 0.632$ and $R_a = 0.219$.

The procedure used in the estimation of the dose from fission-product gammas was to assume that the dose attenuation kernel appropriate to this photon distribution is the same as that appropriate to the prompt fission gamma distribution. This should be a good approximation for our purposes [33]. With this assumption, the leakage calculation for prompt fission gammas had only to be scaled by the factors R_s and R_a displayed above to yield the quantities sought.

* *Private communication with H.D. Brown and D. Newby.*

APPENDIX 3B

STUDIES OF Na^{24} ACTIVATION IN MAN-SHAPED PHANTOMS

3B.1. The Los Alamos burro experiment

An experiment [34] was performed at the Godiva II reactor of Los Alamos Scientific Laboratory to determine whether a phantom composed of a thin shell filled with an aqueous sodium solution could be substituted for a live animal in studies of the relationship between neutron dose and Na^{24} production in the irradiated substance.

A live burro was placed in an aluminium tank, which was then filled with NaCl solution and irradiated at 3 m, centre to centre, from Godiva. Samples of the burro blood serum and of the NaCl solution were prepared, and the Na^{24} activities were determined. The burro was removed, the tank refilled with NaCl solution and an exposure made again at the same position. The NaCl solution was sampled and its Na^{24} activity determined. During the second exposure the region in the tank which had previously been filled by the burro was filled by a homogeneous aqueous NaCl solution. The region was, of course, of the same size and shape when filled with NaCl solution as when filled with the burro. If the amount of Na^{24} produced by the first irradiation was, within experimental error, the same as that produced by the second irradiation, then the production of Na^{24} in a homogeneous phantom could be considered sufficiently similar in quantity to the production of Na^{24} from the Na^{23} heterogeneously distributed in a live animal that phantoms could be substituted for animals.

Concentrations of Na^{24} in the burro and the NaCl solution around it were weighted by the respective volumes and averaged, then compared with the Na^{24} concentration in the full tank of NaCl solution, normalized to the same exposure dose. The relative difference in the amount of Na^{24} produced by the two exposures was 2.9%, which is well within the probable experimental error; hence it was concluded that when a man-shaped phantom is filled with a sodium chloride solution, a good approximation to a man is obtained, insofar as sodium activation is concerned.

TABLE X

Na^{24} CONCENTRATIONS IN MOLDED PHANTOMS

Segment	Na^{24} concentration (μc Na^{24}/mg Na^{23}/rad) × 10^5					
	Calvin I	Remab I	Tyrone I	Calvin II	Remab II	Tyrone II
Head and upper torso	1.44	1.44	1.30	1.55	1.38	1.45
Upper left arm	1.16	1.72	1.75	1.54	1.65	1.82
Upper right arm	1.60	1.28	1.13	1.94	1.45	1.68
Lower left arm	1.18	1.57	1.70	1.78	1.77	1.91
Lower right arm	1.54	1.21	1.17	1.89	1.36	1.84
Lower torso	0.848	0.929	0.781	1.10	0.875	1.01
Gonads	0.842	1.04	1.02	2.08	1.85	1.07
Upper left leg	0.914	1.12	1.16	1.34	1.22	1.23
Upper right leg	1.12	1.03	0.879	1.35	1.27	1.26
Lower left leg	1.13	1.40	1.46	1.60	1.39	1.69
Lower right leg	1.34	1.46	1.18	1.68	1.38	1.63
Average [Mean 1.21]	1.09	1.17	1.09	1.38	1.24	1.28

3B.2. Distribution of Na^{24} in phantoms irradiated at Vinča

Na^{24} concentrations in the phantoms are listed in Tables X and XI. All concentrations are corrected to zero time and are expressed in $\mu c\ Na^{24}/mg\ Na^{23}/rad$. Two tables are given because the two types of phantoms are segmented slightly differently; in both tables the numerals I and II after the name of the phantom indicate first and second high-power exposures, respectively. The molded plastic phantoms in Table X were designated "Calvin", "Remab" and "Tyrone"; the polyethylene bottle phantom in Table XI was called "Bomab". The segments labelled "average" were averaged by mixing and sampling of the total solution of each phantom.

TABLE XI

Na^{24} CONCENTRATIONS IN BOTTLE PHANTOMS

Segment	Na^{24} concentration ($\mu c\ Na^{24}/mg\ Na^{23}/rad$) $\times 10^5$	
	Bomab I	Bomab II
Head	1.40	1.34
Neck	1.33	1.29
Left arm	1.11	1.46
Right arm	1.62	1.58
Upper torso	0.853	1.00
Lower torso	0.755	0.865
Upper left leg	0.846	1.06
Upper right leg	1.11	1.11
Lower left leg	1.03	1.16
Lower right leg	1.25	2.40
Average [Mean 1.045]	0.991	1.10

APPENDIX 3C

INTERCOMPARISON OF FRENCH AND AMERICAN Na^{24} CALIBRATIONS

3C.1. Summary of the Saclay Na^{24} counting method

The total amount of Na^{24} in the bodies of the exposed persons was determined by the French group by means of a scintillation counter. The detector, a 1.5-in × 1-in sodium iodide crystal, was placed at the centre of an arc 1 m in radius. The individual to be measured lay on the floor facing the detector and curved so as to fit just inside the arc. The electronic equipment used in conjunction with this detector consisted of a 25-channel analyser. With the equipment used thus, the response peak from Cs^{137} gamma rays was in the ninth channel and that from K^{40} gamma rays was in the twentieth channel. The activity which was measured in the exposed persons was known from the energy and half-life considerations to be Na^{24}.

The equipment was calibrated with a polyethylene bottle containing Na^{24} solution of known activity. This bottle was moved along the inside of the arc for measurement of the angular dependence of the response of the detector. The size of the bottle (15 cm in diameter, 25 cm in height) was chosen so that the ratio of counts in channels 1-5 to the counts in channels 16-18 was approximately the same whether the activity in the bottle or the activity in the persons was being measured.

3C.2. Studies of the Saclay Na^{24} counting geometry

For confirmation of the method of calibration of the equipment used to measure the Na^{24} activity of the exposed individuals, an experiment was performed at ORNL with a similar crystal, 1.5-in × 1-in sodium iodide. A molded plastic phantom (Remab) and the bottle phantom (Bomab) were filled with a homogeneous aqueous solution of Na^{24} of known concentration. The Na^{24} gamma-ray activity of the phantoms was measured with the same geometry as has been used for measurement of the Na^{24} activity of the exposed persons; i.e., the crystal was at the centre of an arc 1-m in radius, and the phantom was positioned inside the arc, lying on its side on the floor.

The counting efficiency of this geometry was compared with the counting efficiency determined with a polyethylene bottle, 15 cm in diameter and 25 cm in height, filled with Na^{24} solution, placed at various positions inside the 1 m arc. The response of the crystal was found to be independent of the position of the bottle along the arc. Integral measurements were made at energies of 0.366, 0.66 and 1.16 MeV. The ratio of the count rate at 0.366 MeV to the count rate at 1.16 MeV was found to be the same for the two phantoms and for the bottle. The results of this experiment, shown normalized to the counting efficiency for Na^{24} in the bottle, are given in Table XII.

TABLE XII

RELATIVE COUNTING EFFICIENCY FOR Na^{24} IN A BOTTLE AND IN PHANTOMS

Energy (MeV)	Relative counting efficiency		
	Bottle	Remab	Bomab
0.366	1.00	0.984	0.997
0.66	1.00	0.969	0.971
1.16	1.00	0.980	1.00
0.366/1.16	2.66	2.66	2.64

3C.3. Direct intercomparison of Saclay and Oak Ridge Na^{24} counting methods

For comparison of the calibration of the French equipment used to measure the Na^{24} in the bodies of the exposed individuals with the calibration of the ORNL equipment used to determine the Na^{24} concentration in the phantoms, average samples of Calvin II, Remab II and Tyrone II solutions were prepared and sent to Paris for Na^{24} measurements. The results of the French analysis were communicated to us by H. Jammet and L. Jeanmaire on 31 May 1960. An additional solution sample which had been prepared by dissolution of irradiated solid NaCl was included to obtain a higher disintegration rate. Activity concentrations of the solutions are listed in Table XIII.

TABLE XIII

CROSS CALIBRATION OF FRENCH AND ORNL EQUIPMENT FOR MEASUREMENT OF Na^{24} CONCENTRATION

Solution	ORNL value ($\mu c/ml$) × 10^3	French value ($\mu c/ml$) × 10^3	ORNL value / French value
Calvin II	1.06	1.03	1.03
Remab II	1.19	1.16	1.03
Tyrone II	1.09	1.05	1.04
Solution from solid NaCl	33.2	33.9	0.98

APPENDIX 3D

STUDY OF THE NEUTRON FLUX DISTRIBUTION IN THE VINČA REACTOR ROOM

For documentation of neutron data previously given, some of the data from the two high-power runs at Vinča are shown in Figs. 24 through 31. The data presented are from the secondary stations consisting of sulphur, gold and cadmium-shielded gold. Locations of the various stations are shown in Fig. 16.

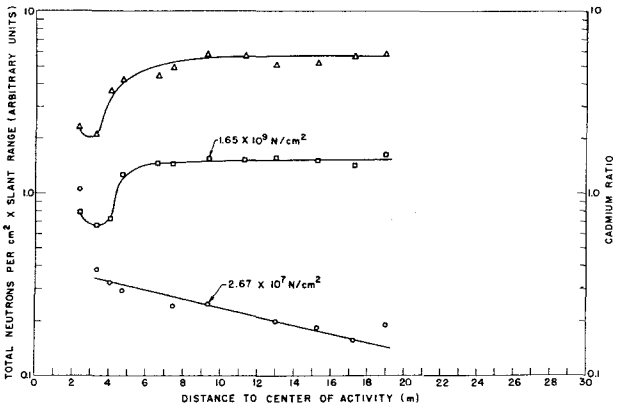

Fig. 24

High-power run No. 1 - line running east through LPS-5, 108 cm from floor.

- ○ Fast neutrons
- □ Thermal neutrons
- △ Cadmium ratio

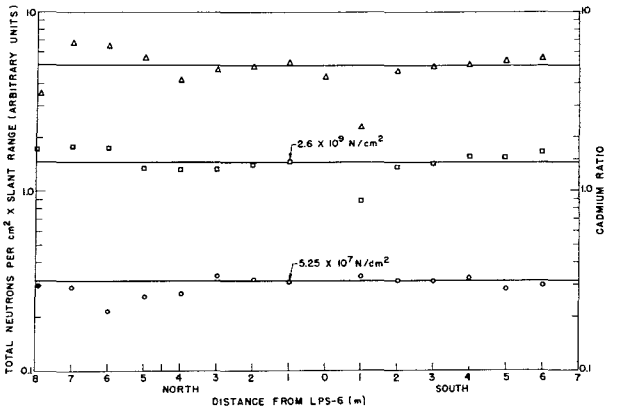

Fig. 25

High-power run No. 1 - horizontal traverse, 108 cm from floor, running north and south through LPS-6.

- ○ Fast neutrons
- □ Thermal neutrons
- △ Cadmium ratio

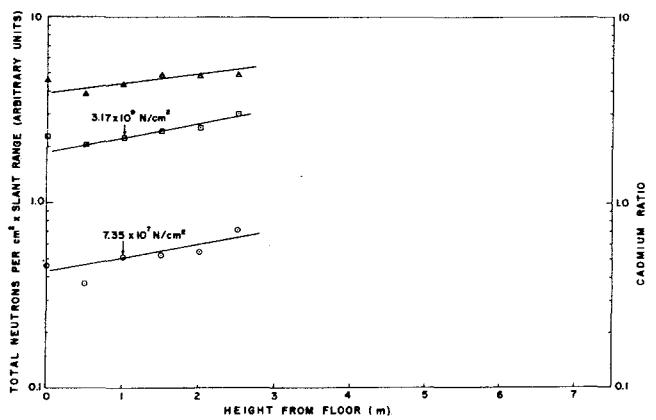

Fig. 26

High-power run No. 1 - vertical traverse at LPS-2.

- ⊙ Fast neutrons
- ⊡ Thermal neutrons
- ◬ Cadmium ratio

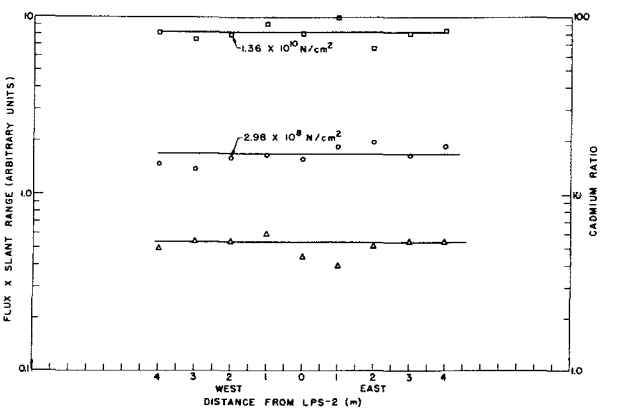

Fig. 27

High-power run No. 2 - horizontal traverse, 108 cm from floor, running east and west through LPS-2.

- ○ Fast neutrons
- □ Thermal neutrons
- △ Cadmium ratio

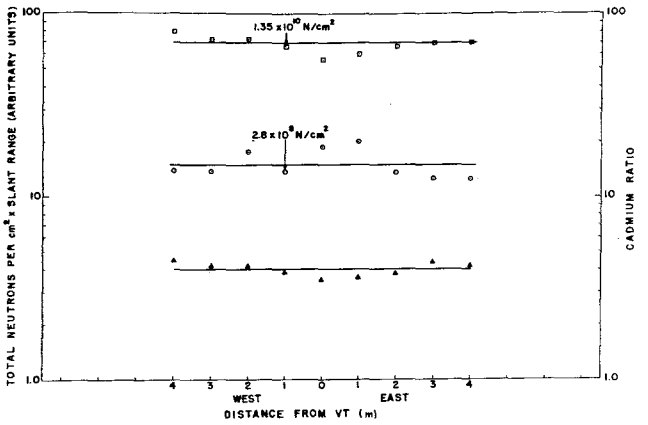

Fig. 28

High-power run No. 2 – horizontal traverse, 108 cm from floor, running east and west through VT.

⊙ Fast neutrons
⊡ Thermal neutrons
△ Cadmium ratio

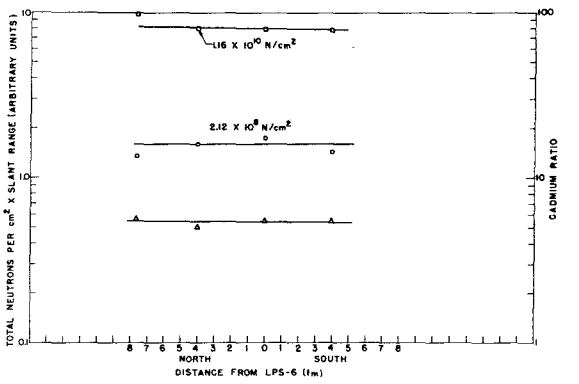

Fig. 29

High-power run No. 2 – horizontal traverse, 108 cm from floor, running north and south through LPS-6.

○ Fast neutrons
□ Thermal neutrons
△ Cadmium ratio

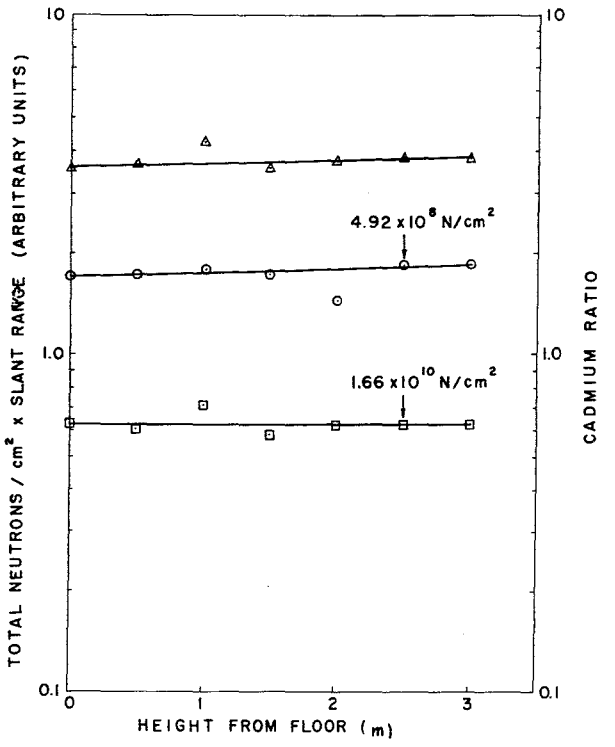

Fig. 30

High-power run No. 2 – vertical traverse through VT.

⊙ Fast neutrons
⊡ Thermal neutrons
△ Cadmium ratio

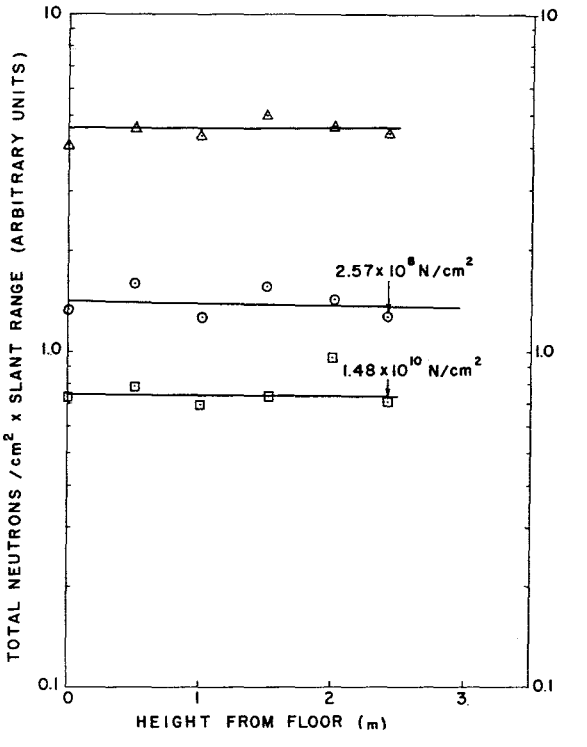

Fig. 31

High-power run No. 2 – vertical traverse 3 m west of VT.

⊙ Fast neutrons
⊡ Thermal neutrons
△ Cadmium ratio